(Preprint) AAS-AIAA

MID-LIFT-TO-DRAG RATIO RIGID VEHICLE 6-DOF EDL PERFORMANCE USING TUNABLE APOLLO POWERED GUIDANCE

Breanna Johnson,[*] Ping Lu,[†] and Christopher Cerimele[‡]

The Mid-Lift-to-Drag ratio Rigid Vehicle (MRV) is a candidate in the NASA multi-center effort to determine the most cost effective vehicle to deliver a large-mass payload to the surface of Mars for a human mission. Products of this effort include six-degree-of-freedom (6DoF) entry-to-descent trajectory performance studies for each candidate vehicle. These high fidelity analyses help determine the best guidance and control (G&C) strategies for a feasible, robust trajectory. This paper presents an analysis of the MRV's G&C design by applying common entry and descent associated uncertainties using a Fully Numerical Predictor-corrector Entry Guidance (FNPEG) and tunable Apollo powered descent guidance.

INTRODUCTION

NASA's Evolvable Mars Campaign was formulated with the goal of defining the strategy and the operational capabilities needed for a human presence further in the solar system, including Mars, starting in the 2030s. One of the great challenges is defining a feasible mission with a vehicle architecture capable of delivering a 20 metric ton (mt) payload to the surface of Mars. This requirement is based on an estimate of the minimum amount of payload required for a Mars Ascent Vehicle (MAV), which would need to be transported for a future return mission. Previous robotic missions to the Mars surface have primarily featured low ballistic entry vehicles with parachutes that deploy at subsonic velocities to ensure a soft touchdown. However, multiple sources have demonstrated that with the current state of the art technology, this approach would be infeasible for a human mission due to the large mass required and low density of the Mars atmosphere. For this reason, the Mid-Lift-to-Drag ratio Rigid Vehicle (MRV) will need to use supersonic-retro-propulsion (SRP) in its descent and landing phases of flight.

Robotic and even human missions have utilized some version of the heritage Apollo Entry guidance to achieve soft touchdown and precision landing, such as the Mars Science Laboratory (MSL) and Orion vehicles.[1, 2] A human mission to Mars would require an even smaller footprint from the recent MSL landing ellipse of 25x20 km,[3] as well as experience smaller peak g-loads than the previous MSL robotic mission. Typical human safety requirements for human missions are limited to 4 g's for a deconditioned crew, but the MSL mission saw nominal peak loads of up to 10 g's.[1] For these reasons, the entry, descent, and landing (EDL) guidance and control (G&C) strategy for a human mission to Mars must be capable of providing soft and precision landing, while abiding human safety constraints.

[*] Aerospace Engineer, Flight Mechanics and Trajectory Design Branch NASA JSC/EG5.
[†] Professor and Chair, Department of Aerospace Engineering; plu@sdsu.edu, Fellow AIAA.
[‡] EDL Domain Lead, Aerosciences and Flight Mechanics Division, NASA JSC/EG5.

METHODOLOGY

The JSC Flight Analysis and Simulation Tool (FAST) is used to develop and simulate both the 3DoF and 6DoF EDL solution. Previous 6DoF EDL simulation results used a vehicle shape generated by the Co-Optimization Bluntbody Re-entry Analysis (COBRA) tool to optimize aerodynamic and aerothermal properties by changing the Outer Mold Line (OML) of the MRV.[4] These methods were again employed to update the vehicle properties from the CobraMRV 2908b to the CobraMRV 2908g OML. With this update, the vehicle entry mass of 58.7 mt also increased to 61.8 mt. Improvements to the design included smoothing the transition from the fuselage to the flap hinge line, in order to reduce flap heating, as well as increased fidelity in structural modeling. Although there have been updates to the vehicle structure to increase fidelity and aerodynamic characteristics, Figures 1 and 2 show that the overall dimensions of the main body remain at 19.8 m in length, 8.8 m in width, and 7.3 m in height.

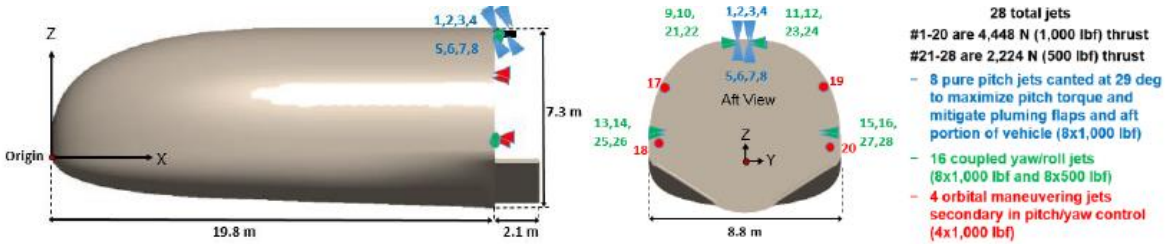

Figure 1. CobraMRV 2908b and RCS Jet Locations.

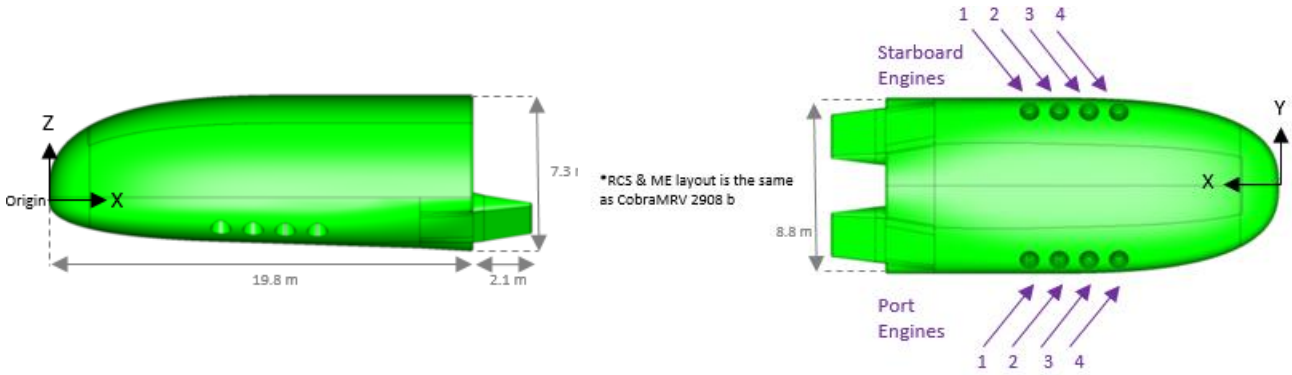

Figure 2. CobraMRV 2908g and Main Engine (ME) Jet Locations.

Similarly, the CobraMRV 2908g maintains an aerodynamic reference length of 19.8 m, a surface area of 160 m^2, a hypersonic L/D ratio of 0.54, and a ballistic coefficient of 379 kg/m^2 at entry. A total of twenty-eight 4,448 N and 2,224 N Reaction Control System (RCS) thrusters are used in conjunction with the split body flaps in order to provide trimming capabilities to reduce jet firings and bank angle modulation throughout entry. Eight 100 kN main engines are used with RCS for the descent and landing phases of flight to provide trim management and follow throttle commands.

Due to the expected ineffectiveness of the flaps with the main engines on, the RCS is used during powered descent and landing. To test that the G&C strategy is robust, vehicle candidates must meet g-load and heating constraints not only for a nominal trajectory, but must also meet these constraints even when various EDL dispersions and uncertainties are applied. Therefore a successful Monte Carlo analysis would result in maximum g-loads below 4 g's, soft landing (velocities below 5 m/s), and a landing footprint of no more than 10m. Heating rates should be in family of what is expected for a Thermal Protection System (TPS) comprised of ablators and Shuttle derived

flexible blankets (50-60 W/cm^2).[4] This paper will assess the G&C strategy of using a Fully Numerical Predictor-corrector Entry Guidance (FNPEG) in conjunction with the newly developed Tunable Apollo Powered Descent Guidance (TAPDG) [5] to meet these constraints.

Entry Guidance and Control Overview

FNPEG, like heritage entry guidance algorithms, generates bank angle commands which serve to modulate the direction of the lift vector, such that the distance to the target is minimized and the vehicle is guided to a user-specified energy, as defined in Equation 1.[6]

$$e = \frac{1}{r} - \frac{V^2}{2} \tag{1}$$

In order to reduce stress on the RCS and save propellant, the commanded angle of attack and sideslip angles are set at the vehicle's natural aerodynamic trim stability points, based on the expected location of the center of gravity (CG). The magnitudes of the guided bank angle commands follow a linear profile with energy, as shown in Figure 3, where ϕ_0 represents the vehicle's current bank angle and normalized energy and where ϕ_f is a user defined constant defined a priori that may be tuned to improve robustness to dispersions.[7]

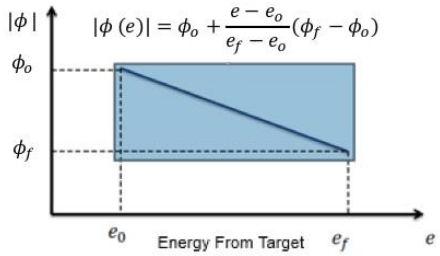

Figure 3. Linear bank angle profile with energy.

The predicted bank angle command profile shown in Figure 3 is generated based on the current state at each guidance step in addition to the solved translational and rotational equations of motion that are used to predict the full trajectory. If the predicted trajectory does not reach the target at the user defined energy, ϕ_0 is corrected through an iterative Gauss-Newton method solver until the range to target (s) error function, as defined in as defined in Equation 2, is minimized.[6]

$$f(\phi_0) = \frac{1}{2}\left[s(e_f) - s_f^*\right]^2 \tag{2}$$

Bank angle modulation is primarily achieved with the twenty-eight engines shown in Figure 1, while trim stability is primarily maintained with the split body flaps located at the aft of the vehicle, serving as the coupled rudder and elevon. The classical control algorithm used in entry determines the gains required based on the current estimated dynamic pressure and the desired augmented frequency in the longitudinal and lateral directional axes.[8] In order to achieve the desired system response in accordance with Equations 3 and 4, gains may be derived from Equations 5-7 in order to determine appropriate proportional and derivative gains.

$$\ddot{\alpha} + 2\xi\omega_{SP}\dot{\alpha} + \omega_{SP}^2\alpha = 0 \tag{3}$$

$$\ddot{\beta} + 2\xi\omega_{DR}\dot{\beta} + \omega_{SP}^2\beta = constant \tag{4}$$

$$\tau_x = I_x\dot{p} = C_{l_\beta}\beta\bar{q}SL + m_x\left(-K_\beta\beta - K_p p + K_p r_c cot\alpha\right) + C_{l_{\delta_a}}\delta_a\bar{q}SL \tag{5}$$

$$\tau_y = I_y\dot{q} = C_{m_\alpha}\alpha\bar{q}SL + m_y\left(K_\alpha(\alpha_c - \alpha) - K_q q\right) + C_{m_{\delta_e}}\delta_e\bar{q}SL \tag{6}$$

$$\tau_z = I_z\dot{r} = C_{n_\beta}\beta\bar{q}SL + m_z(K_r r_c - K_r r) + C_{n_{\delta_a}}\delta_a\bar{q}SL \quad (7)$$

The CobraMRV design updates also led to an update in the targeted X_{CG} (10.54 m to 10.47 m) as defined in the Figure 1 coordinate system and a reduction in flap actuation rate limits (30 deg/s to 10 deg/s). Figure 4 shows the nominal trajectories, starting at an altitude of 125 km and velocity of 4.7 km/s heading north. The relative entry flight path angle is chosen at -10.2 deg and the atmosphere is modeled with MarsGRAM 2010. The Lagrangian 85x85 gravitational field is applied.

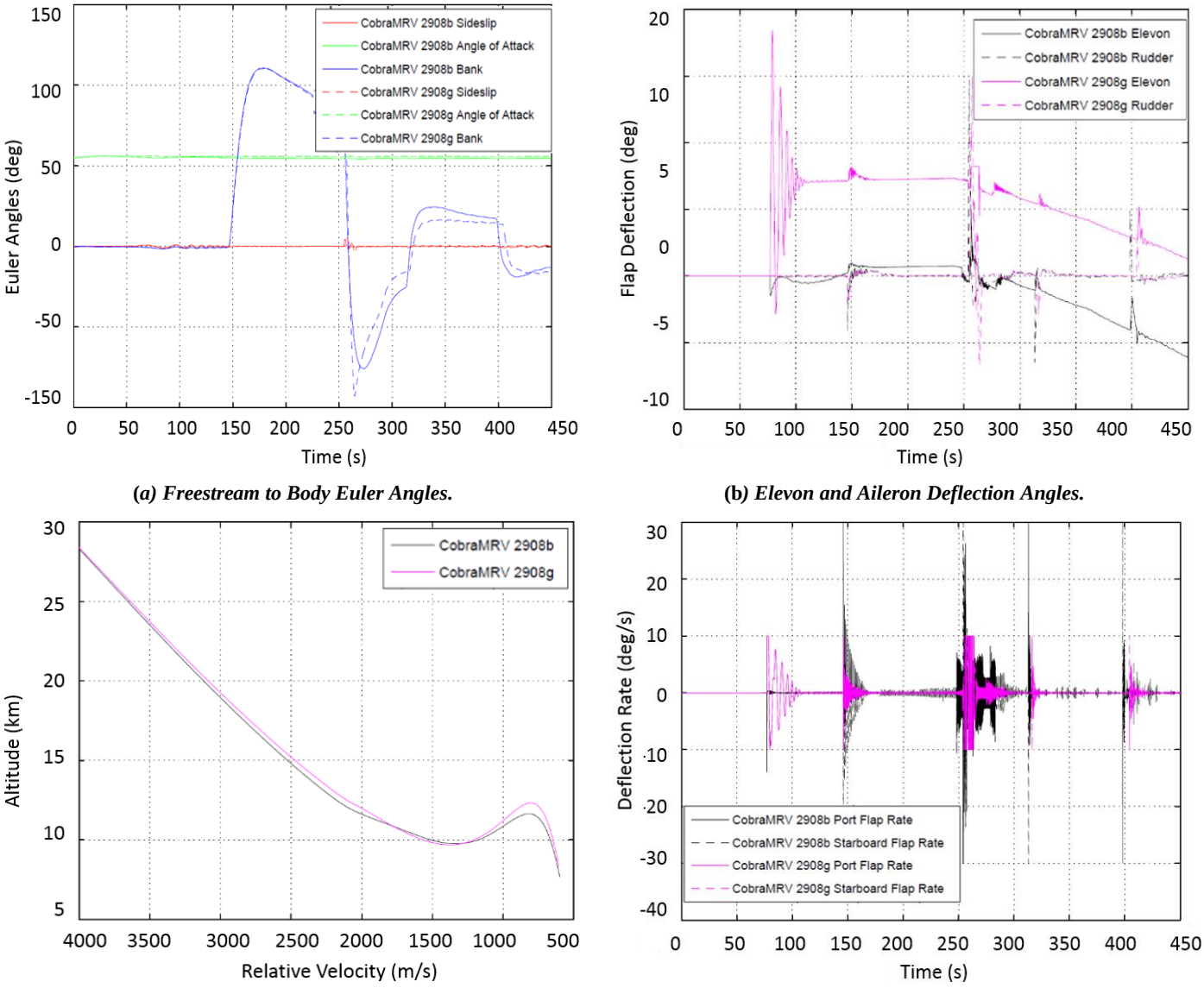

(a) Freestream to Body Euler Angles.

(b) Elevon and Aileron Deflection Angles.

(c) Energy Profiles.

(d) Starboard and Port Flap Rates.

Figure 4. CobraMRV2908b and CobraMRV2908g Trajectory Comparison.

In this nominal trajectory, the angle of attack and sideslip angles maintain their 55 deg and 0 deg trim conditions, respectively, within their prescribed dead bands. The bank angle stays within its 1 deg deadband throughout flight and achieves the prescribed three bank reversals. And as expected, the energy profile remains to be very similar between the two CobraMRV models. A preliminary analysis of the flap actuator mechanism, estimated mass properties, and power requirements was

done based on similar assumptions used for the Shuttle orbiter. For this heavier vehicle, a trade study on scaling up the actuators revealed that the new left and right flap rates should not exceed 10 deg/s until further work is completed. Thus this limitation was included in the updated 6DoF simulation as shown in Figure 4. Both CobraMRV 2 908b and CobraMRV 2908g simulated trajectories yield satisfactory bank angle tracking and entry termination point targeting. The change in X_{CG} was implemented to effectively improve yaw and pitch stability during entry. This change increases the trim nominal elevon deflection from 0 deg to 8 deg, also shown in the comparison plots of Figure 4b. Aileron trim deflection remains at 0 deg.

A CG box had been previously defined for the MRV, based on expected possible CG uncertainties that could be present at launch.[9] This box was defined as $\pm$ 20 cm in X, $\pm$ 5 cm in Y, and $\pm$ 20 cm in Z. Previous stability analyses show that for mid-L/D geometries, the vehicle is most resistant to CG uncertainty in Z and most vulnerable in Y. Figure 5 shows that if there is a maximum X_{CG} and Cm uncertainty biasing the vehicle to pitch up, the elevon would trim at a more positive value of 20 deg in order to produce a negative pitching moment to counteract the disturbance. The updated nominal X_{CG} and nominal elevon deflection of 8 deg also improved coverage of the longitudinal CG box, such that maximum elevon deflections of $\pm$ 20 deg, can sufficiently eliminate destabilizing moments from $\pm$20 cm X_{CG} offsets. In fact, designated pitch RCS jets are consistently the least active of all RCS jets, as shown in Figure 5.

Similarly, rudder deflections of $\pm$ 15 deg, can sufficiently eliminate destabilizing moments from $\pm$5 cm Y_{CG} offsets. Figure 5 also illustrates the vehicle response to a lateral worst case offset if Y_{CG} is moved 5 cm starboard. This worst case also coupled maximum estimated rolling moment uncertainties. The controllability in the face of these uncertainties highlight the vehicle's robustness to the common issues that often hurt vehicles of the mid-L/D class. Due to the vehicle's asymmetry, moments induced by the CG offset from nominal in the Y direction may be naturally trimmed only with a combination of rudder deflection and non-zero sideslip angle. It is for these reasons, a sideslip angle deadband of 10 deg was chosen to allow for equilibrium to be reached even in the event of a maximum Y_{CG} offset. The angle of attack deadband is tighter at 1 deg about trim due to better trim capabilities of the elevon, as compared to the rudder, and better overall static stability.[8]

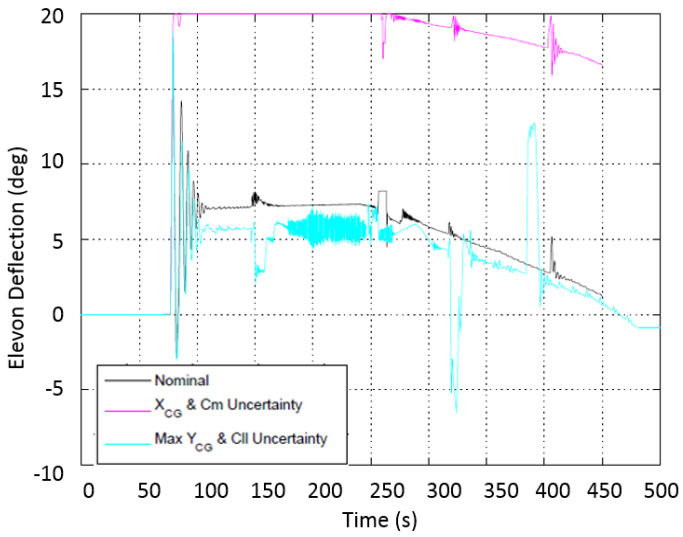

(a) Elevon Deflection vs. Time.

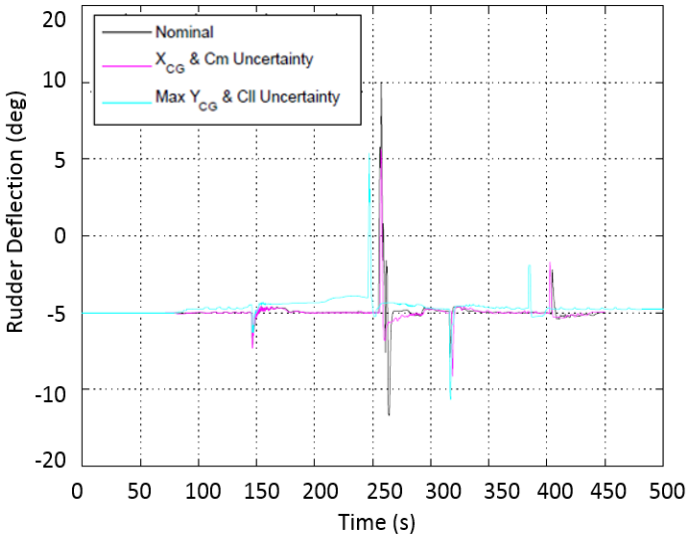

(b) Rudder Deflection vs. Time.

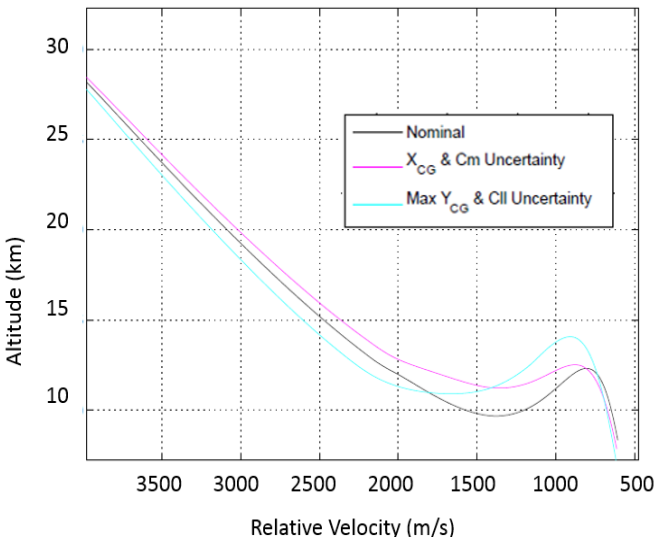

(c) Energy Profile.

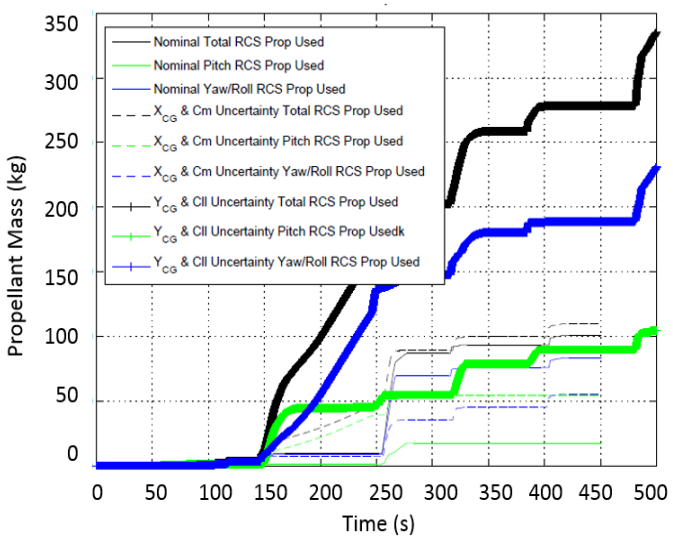

(d) Propellant Used per Axis vs. Time.

Figure 5. CobraMRV 2908g Nominal vs. Maximum Aerodynamic & CG Uncertainty Comparison.

Descent and Landing Gravity Turn Guidance and Control Overview

Ensuring that the descent and landing phase is as close to fuel optimal as possible is desired for a human Mars mission to reduce costs and maximize payload mass. And while global fuel optimality is desirable, realistic engine design constraints and uncertainties limit feasible optimal powered descent guidance strategies, which prompt the desire for a throttle and energy profile that can be shaped. Previous analysis shows that while an open-loop simple constant thrust gravity turn may be near propellant optimal for a nominal trajectory, it sacrifices in robustness to dispersions at engine startup and would inherit any position error from entry dispersions. Conversely, constant acceleration analytical closed-loop gravity turns have some increased robustness to dispersions to achieve soft landing, but typically require more fuel.[9] While gravity turns allow for soft landing trajectories with simplified guidance logic, gravity turn options have shown poor performance in precision landing due to the fact that the primary objective of a gravity turn is to achieve a soft landing. This is evidenced by a lack of a position consideration in the closed loop analytical gravity turn guidance law defined by Equation 8.[9]

$$\left(\frac{a_T}{g}\right)^2 + sin\,\gamma_0\,\left(\frac{V_0^2}{2h_0 g}\right)\frac{a_T}{g} - \left[\frac{V_0^2(1+\sin^2\gamma_0)}{4h_0 g} + 1\right] = 0 \qquad (8)$$

The TAPDG guidance law is an improvement from previous studies using a constant acceleration gravity turn due to its near propellant optimal solutions and flexibility. While the Apollo lunar descent guidance has no free parameter to tune, the recently developed TAPDG allows the user to adjust a gain k_r to either achieve a near propellant-optimal trajectory, or shape the powered descent trajectory. The TAPDG law is given by [5]

$$\boldsymbol{a_T} = \frac{2}{t_{go}}\left(1 - \frac{1}{3}k_r\right)\left[\boldsymbol{V_f^*} - \boldsymbol{V(t)}\right] + \frac{k_r}{t_{go}^2}\left[\boldsymbol{r_f^*} - \boldsymbol{r(t)} - \boldsymbol{V(t)}t_{go}\right] + \frac{1}{6}(k_r - 6)\boldsymbol{a_{T_f}^*} + \frac{1}{6}(k_r - 12)\boldsymbol{g} \qquad (9)$$

For different values of $k_r$the TAPDG law family include both heritage Apollo lunar descent guidance and E-guidance as special cases.[5] Specifically, when the k_r gain is set to 12, the TAPDG law becomes the familiar Apollo lunar descent guidance,[5] and the value of 6 for k_r in Equation 9 will give rise to the E-guidance.[10]

Figure 6 compares the 6DoF profiles of a nominal TAPDG and a nominal constant acceleration gravity turn guided decent. As expected, the constant acceleration case achieves a soft landing with poor targeting performance. In TAPDG cases, the targeting consistently achieves sub-meter accuracy, a soft landing, and propellant usage that increases with increasing k_r. The thrust profiles demonstrate the non-linear nature of the TAPDG guidance compared to the more linear constant acceleration closed-loop gravity turn profile. This trend is also observed in the altitude vs velocity profiles where the higher k_r gained case consumes more propellant with the more conservative approach (lower velocities than the lower k_r case at the same altitudes).

While the TAPDG algorithm offers the user the ability to essentially change the energy profile of the descent trajectory and has benefits compared to some gravity turn and fuel optimal descent guidances, the user would still need to define a time-to-go (t_{go}) and powered descent initiation (PDI) condition before the SRP phase begins. Typically these values are found through trial and error and are strongly tied to a reference trajectory. However, it may also be shown that best values for t_{go} and PDI conditions may be found using a sweep of different range-to-go triggers.

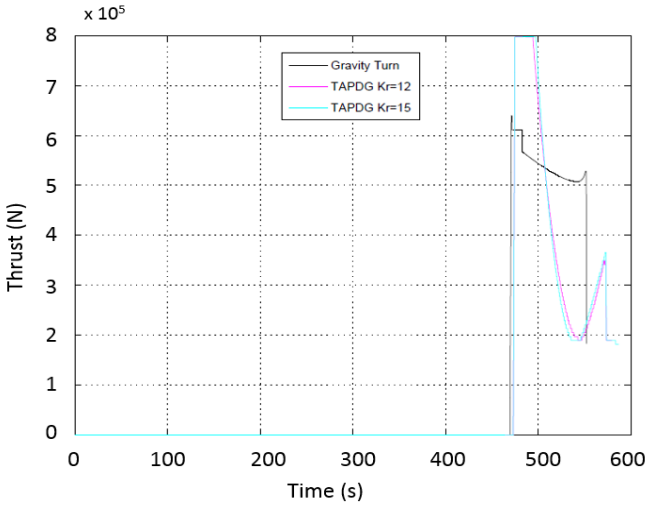

(a) Thrust Profiles for Gravity Turn and TAPDG.

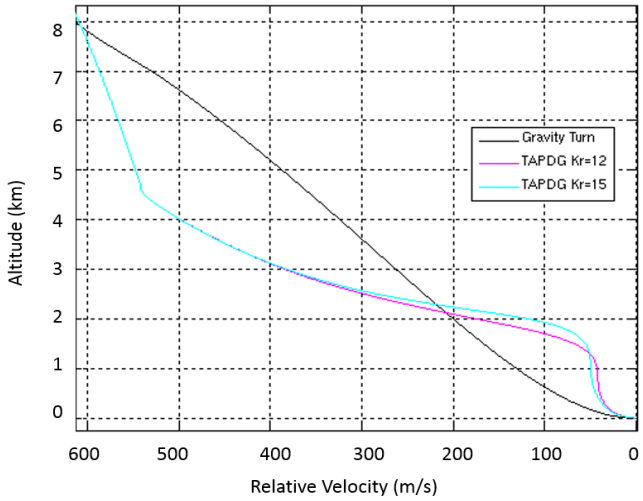

(b) Energy Profiles for Gravity Turn and TAPDG.

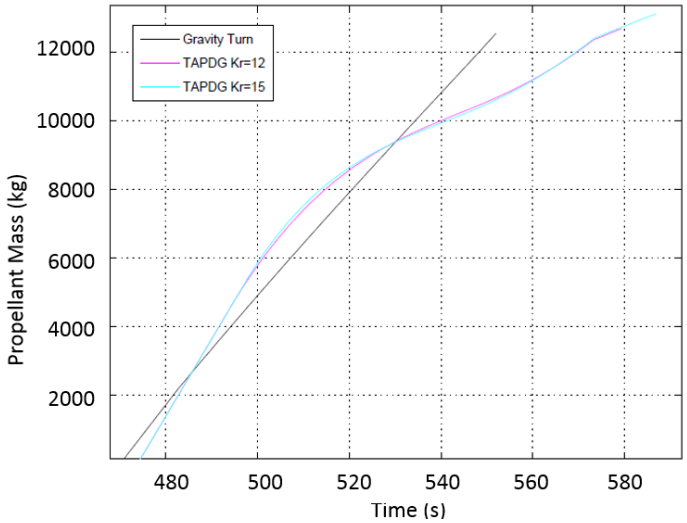

(c) Propellant Mess Used for Gravity Turn and TAPDG.

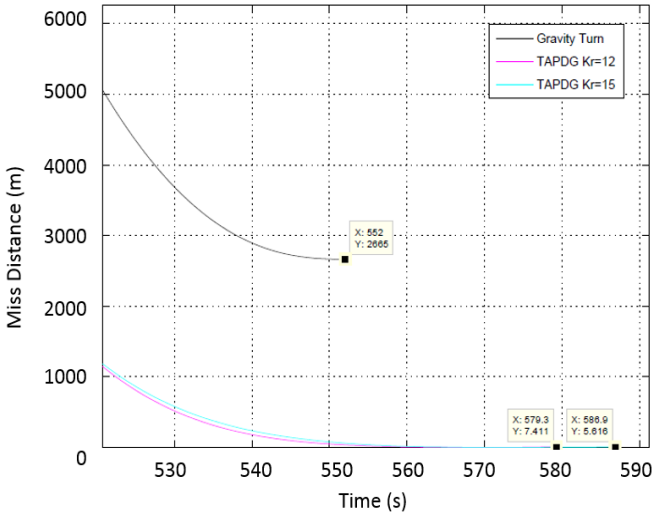

(d) Miss Distance for Gravity Turn and TAPDG.

Figure 6. Powered Descent Guidance Law Comparison.

Figure 7 illustrates that the likely best combination of range-to-go and time-to-go triggers until engine cutoff are between 15 and 17 km, due to the consistently accurate termination of entry and descent at the user specified altitude of 12.5 m and 2.5 m/s for both 3DoF and 6DoF sweeps.

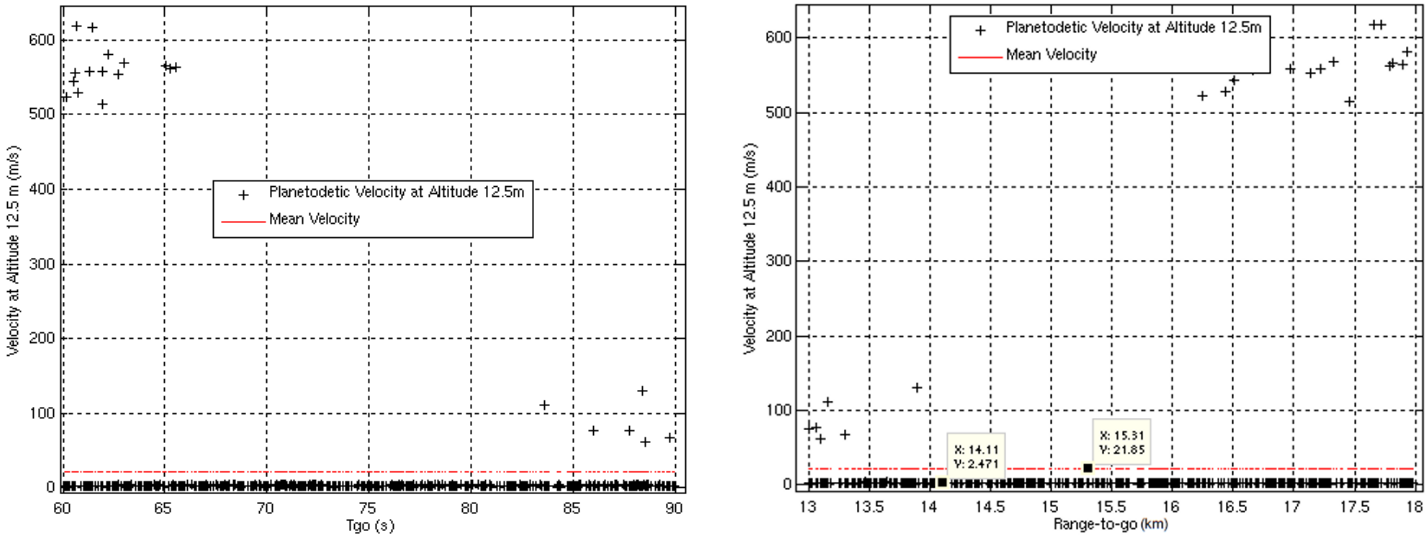

(a) Velocity at TAPDG Termination vs. Time-to-go Inputs. *(b) Velocity at TAPDG termination vs. Range-to-go Inputs.*

Figure 7. Range-to-go and Time-to-go Sweeps for TAPDG.

Sweeps of t_{go} and range-to-go may be performed before Monte Carlo analyses to estimate the best combinations to give satisfactory results. For this study, FNPEG terminal energy targets of 2 km altitude and 350 m/s velocity were chosen to deplete the high energy from entry as much as possible before PDI in order to reduce the needed main engine on-time. However, trade studies have shown that a chosen FNPEG terminal energy may not necessarily be the best PDI condition. In fact, the most favorable PDI conditions are also highly dependent upon the powered descent guidance chosen.

Currently, simulations of the EMC vehicle candidates also have a vertical descent phase beginning at an altitude of 12.5 m and velocity of 2.5 m/s, allowing for improved navigation estimates and autonomous landing hazard and avoidance technology capabilites[8] to improve state inputs to guidance. While navigation algorithms and their applications are not covered in this paper, including the vertical descent phase will aid in future guidance, navigation, and control robustness studies. This vertical descent phase also encourages a desire for trajectory shaping as the vehicle and the mission mature. It is for this reason that the Monte Carlo results will target an altitude of 12.5 m and velocity of 2.5 m/s to assess only the TAPDG performance, since a simple gravity turn would follow for the last few seconds of flight. Trajectory shaping, changing the rate of descent with respect to the ground range before the vertical descent transition altitude, provides a powerful tool in studies analyzing the fully guidance, navigation, and control solutions. Control of the trajectory shape has also been shown to aid in 6DoF challenge cases, where inherent errors from entry and rate limits impede performance. Therefore the trajectory shaping feature that TAPDG offers would likely increase the robustness to engine startup times, engine startup dispersions, throttle keep-out zones, and center of gravity uncertainties that are not typically explored with fuel optimal powered descent solutions.

MONTE CARLO RESULTS

Previous work with the Mid-Lift-to-Drag ratio Rigid Vehicle (MRV) has shown that a hypersonic vehicle with a mid-lift-to-drag ratio (mid-L/D) can produce a nominal entry trajectory capable of meeting the human mission design derived constraints of less than 4 Earth g's and less than 5 km targeting error above the landing site.[4, 8] However, an entry-to-landing analysis of the MRV's response to dispersions would better address whether the guidance and control strategies previously presented are viable solutions to the human Mars EDL problem.

Results of the Entry FNPEG footprint

Entry Monte Carlo dispersions include the uncertainties of aerodynamic coefficients (CA, CY, CN, Cl, Cm, and Cn), mass/inertia/CG properties, Mars GRAM dispersions, and entry interface condition dispersions (azimuth, flight path angle, latitude, longitude, altitude). The applied dispersions for entry are listed in Table 1.

Table 1. Entry Interface Dispersions for the Monte Carlo Simulations.

Monte Carlo Varied Parameter	**Distribution**	**3σ / maximum**	**-3σ / minimum**
Altitude (km)	Gaussian	1.00E-01	-1.00E-01
Longitude (deg)	Gaussian	2.50E-01	-2.50E-01
Latitude (deg)	Gaussian	2.50E-01	-2.50E-01
Velocity (m/s)	Gaussian	3.30E+00	-3.30E+00
Flight Path Angle (deg)	Gaussian	1.00E-01	-1.00E-01
Azimuth (deg)	Gaussian	1.70E-01	-1.70E-01
Mass (kg)	Gaussian	2.00E+02	-2.00E+02
CA,CN (%)	Uniform	10%	-10%
CY, Cll, Cm, Cln	Uniform	~ 3 deg	~ -3 deg
Atmospheric density	Mars GRAM 2010	Mars GRAM 2010	Mars GRAM 2010
Mars GRAM 2010 *dusttau*	Uniform	0.9	0.1

Estimated aerodynamic uncertainties were applied according to Equations 10 to 15, where U^m represents a multiplier applied to increase the uncertainty of an aerodynamic database and U^a represents an added uncertainty to the aerodynamic database. Note that MRC refers to the Moment Reference Center.

$$C_A = C_{A,base} + C_{A,base} * U_{C_A}^m + \Delta C_{A_{Flaps}} \quad (10)$$

$$C_Y = C_{Y,base} + U_{C_Y}^a + C_{Y_{\delta_r}} \delta_r \quad (11)$$

$$C_N = C_{N,base} + C_{N,base} * U_{C_N}^m + \Delta C_{N_{Flaps}} \quad (12)$$

$$C_{l_{CG}} = \left[C_{l,MRC} + C_Y \frac{\Delta z}{L_{ref}} + C_N \frac{\Delta y}{L_{ref}} \right] + U_{C_l}^a + C_{l_{\delta_r}} \delta_r \quad (13)$$

$$C_{m_{CG}} = \left[C_{m,MRC} + C_A \frac{\Delta z}{L_{ref}} - C_N \frac{\Delta x}{L_{ref}} \right] + U_{C_m}^a + \Delta C_{m_{Flaps}} \quad (14)$$

$$C_{n_{CG}} = \left[C_{n,MRC} - C_A \frac{\Delta y}{L_{ref}} - C_Y \frac{\Delta x}{L_{ref}} \right] + U_{C_n}^a + C_{n_{\delta_r}} \delta_r \quad (15)$$

Due to the lack of wind tunnel testing and higher fidelity Computational Fluid Dynamics (CFD) work, each coefficient that is zero at trim conditions was added with an estimated ± 3 deg uncertainty (at maximum) for the Monte Carlo simulations. Thus the bounds for these uncertainty terms in Equations 10-15 may be described by the following:

$$U_{C_A}^m = \mathrm{x} \in [-0.1, +0.1]$$

$$U_{C_Y}^a = \mathrm{x} \in [-1, +1] * U_{C_{Y,max\beta}}^a$$

$$U_{C_N}^m = \mathrm{x} \in [-0.1, +0.1]$$

$$U_{C_l}^a = \mathrm{x} \in [-1, +1] * U_{C_{l,max\beta}}^a$$

$$U_{C_m}^a = \mathrm{x} \in [-1, +1] * U_{C_{m,\max\ \alpha}}^a$$

$$U_{C_n}^a = \mathrm{x} \in [-1, +1] * U_{C_{n,max\beta}}^a$$

Each uncertainty adder's maximum value is provided in Table 1. Once better aerodynamic CFD-derived uncertainty becomes available, the new databases will replace these estimates. Note that the CY uncertainty uses an adder term, instead of the multiplier used for CA and CN, since at trim conditions, this force coefficient is zero.

While constraint enforcement on maximum g-load and heating rate is an FNPEG feature, the nominal and dispersed results did not need to enable these constraints. The FNPEG entry footprint closely matched 3DoF performance consistent with previous work. Figure 8 shows that the latitude vs longitude errors (miss distances) for a 1,000 run Monte Carlo resulted in all cases reaching the target within the expected 5 km radius. The targeted radius at the end of entry is less stringent than the targeted radius at the ground (10 m), as it is assumed that the powered descent and landing phase should be able to clean up errors gained during entry. It is also shown in Figure 8 that the worst case in miss distance, at approximately 3 km range error, is correlated to high rolling moment and Y_{CG} uncertainty. Before the CobraMRV 2908g update, cases like these were unable to reach the target within this radius due to the further aft X_{CG} target and weaker yaw and roll stability of the fuselage and flap system.

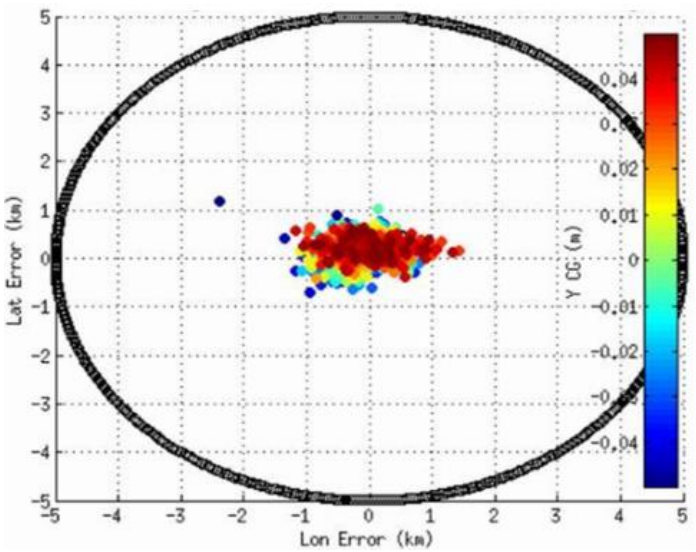

(a) Accuracy at FNPEG Terminal Energy vs. Y_{CG} Uncertainty.

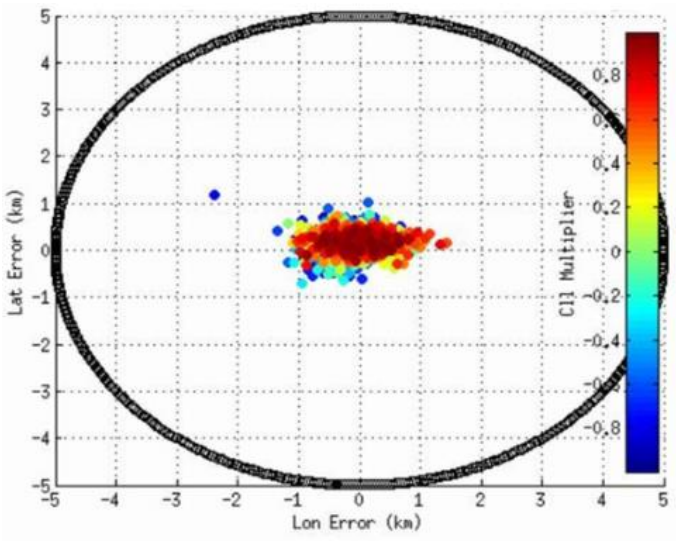

(b) Accuracy at FNPEG Terminal Energy vs. Rolling Uncertainty.

Figure 8. Miss Distance at FNPEG Terminal Energy Condition.

This case was also deemed successful, as the TPS heating constraints remained within 50-60 W/cm^2 and g-load constraints of less than 4 g's was met, as shown in Table 2.

Table 2. Monte Carlo Simulation Results at FNPEG Terminal Energy Condition.

Parameter	Mean	Standard Deviation	Maximum	Minimum
Distance to Target (km)	4.43E-01	2.46E-01	2.82 E+00	1.94 E-02
Velocity (m/s)	5.24 E+03	6.59 E+00	5.71 E+02	5.04 E+02
Max G-load (g)	2.52 E+00	1.68 E-01	3.13 E+00	2.13 E+00
Max Heat Load (kJ/cm^2)	7.23 E+00	2.52 E-01	7.96 E+00	6.61 E+00
Max Heat Rate (W/cm^2)	5.39 E+01	1.66 E+00	5.96 E+02	4.97 E+02
Max Dynamic Pressure (kPa)	8.33 E+00	7.70 E-01	1.14 E+01	6.40 E+00

After satisfactory performance was observed for the 6DoF FNPEG guided entry, the next step was to test the full EDL solution to ensure that the powered descent guidance and control system could truly correct the errors in targeting from entry.

Results of the EDL footprint and performance matrices for all descent guidances

The dispersions applied for the EDL Monte Carlo include those listed in Table 1 as well as powered descent associated dispersions. The challenging dispersions in powered descent include CG offset uncertainties (same as from entry), limited throttle rates (80%/s), main engine startup transients (55%/s), and maximum thrust uncertainties ($\pm 1\%$ 3σ).[9] It should be noted that the descent and landing phases have no applied aerodynamics, as the CFD work is ongoing for the MRV. Thus the descent and landing phases of flight presented here should be more conservative in the amount of propellant needed to achieve a soft landing than if these databases were included. After scanning various t_{go} inputs, k_r gains, and range-to-go triggers, inputs of 75 s for t_{go}, 12 for k_r, and 15 km range-to-go were chosen for the 6DoF EDL Monte Carlo.

Figure 9 shows that the footprint for a 150 case Monte Carlo was much smaller than the required 10 m accuracy. However there is room for improvements, as 2 cases were unable to meet the soft touchdown and footprint constraints using the static inputs provided. Other important statistics about the EDL Monte Carlo performance are included in Table 3.The likely cause of these failed cases is due to range-to-go and t_{go} inputs that are not satisfactory for the given off-nominal cases. Thus another Monte Carlo assessment will need to be performed using the Universal Powered Guidance (UPG) trigger, instead of range-to-go, which would calculate the optimal PDI onboard.[6, 9] Improvements in the targeting accuracy for challenge cases have been observed in 3DoF[6] when using the UPG trigger, but will need to be tested in 6DoF to claim a complete success rate. More work will also need to be done to ensure that similar accuracies can be observed once main engine aerodynamic coefficients are generated and applied to this work. Due to the complexity of the engine to engine plume interaction and high angles of attack, a CFD simulation would be needed to begin capturing these aerodynamics, and is currently in work. Nonetheless, the results shown in Figure 9 certainly provide great insight into the precision and accuracy possible, even when the EDL trajectory is exposed to a multitude of expected vehicle, engine, and aerodynamic dispersions.

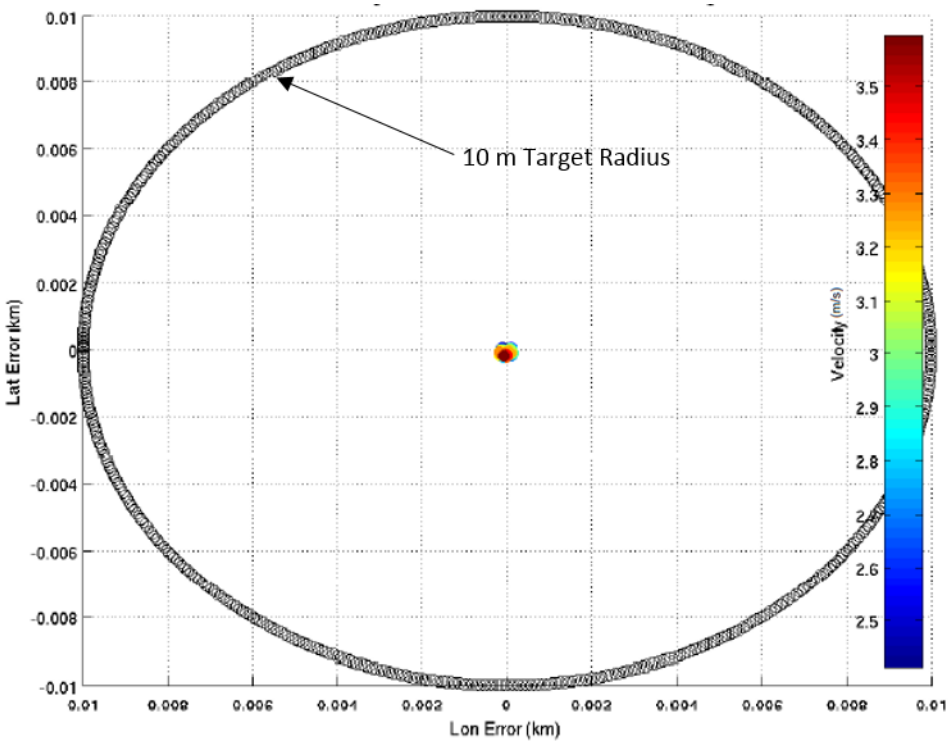

Figure 9. Miss Distance at TAPDG Target (12.5 m Altitude, 2.5 m/s Vertical Descent Rate).

Additionally, it should be investigated at what time the constant acceleration phase of TAPDG should begin (typically less than 5 seconds) to better target 2.5 m/s, since the trajectories were also sensitive to this parameter. These cases should be investigated to determine if the primary contributing factor was improper t_{go} and range-to-go selection or control system inefficiencies.

Table 3. Monte Carlo Simulation Results at TAPDG Target of 12.5 m Altitude.

Parameter	Mean	Standard Deviation	Maximum	Minimum
Miss Distance (m)	1.25E-01	4.62E-02	2.43E-01	0.00E+00
Descent Rate (m/s)	2.88E+00	2.45E-01	3.60E+00	2.42E+00
Propellant Used (kg)	1.16E+04	4.10E+02	1.29E+04	1.07E+04

CONCLUSION

The results of entry, descent, and landing trajectories using FNPEG and TAPDG have been presented in 3DoF and 6DoF. Nominal and off-nominal 6DoF entry cases have been presented to illustrate the difficulties in attaining a 10 m radius footprint on the ground with low velocity. While all entry dispersed trajectories met the expected 5 km radius at the FNPEG termination energy, a small percentage of powered descent cases failed to meet the 10 m radius footprint on the ground. More work will need to be done to assess the best TAPDG inputs to achieve the same level of success shown in 3DoF. However, the results are promising that 100% success is achievable, since each case that landed softly reached the target with sub-meter accuracy. The targeting accuracy and

precision of all successful TAPDG cases is consistent with the successful 3DoF Monte Carlo simulations. The trajectory results imply that the control system approach of using aerosurfaces, main engines, and RCS jets provide an effective strategy for a human Mars MRV mission. These results achieve a major milestone in the EMC study. Future work includes adding engine shutdown transient effects, throttle keep-out zones, and a main engine aerodynamic database formulated by the aerodynamics team at the NASA Langley Research center. More descent and landing work will need to be done to better assess the full TAPDG range of performance, especially with UPG trigger logic. The work presented demonstrates that a feasible trajectory in landing a 20 mt payload to the surface of Mars within 10 m in the face of EDL dispersions is achievable. A future analysis of these results with navigation errors will be completed to show how this accuracy degrades for a full Guidance, Navigation, and Control solution.

ACKNOWLEDGMENTS

The authors acknowledge all the individuals who contributed to this effort. We would like to extend gratitude to Ronald Sostaric, Phil Robinson, Joseph Garcia, Daniel Matz, Kenneth Wong, Ellen Braden, Damien Calderon, Carlos Gaytan, Dave Kinney, Stan Bouslog, Chuck Campbell, Alicia Cianciolo, Tara Polsgrove, and Francis Monahan. We appreciate your guidance and expertise.

NOTATION

a_T	=	commanded thrust acceleration
C_A, C_Y, C_N	=	aerodynamic axial, side, and normal force coefficients
C_l, C_m, C_n	=	aerodynamic rolling, pitching, and yawing moment coefficients
g	=	acceleration due to gravity
h_0	=	height at the start of the gravity turn
e	=	energy used in FNPEG
K	=	control system gain
L_{ref}	=	aerodynamic reference length
M	=	Mach
r	=	vehicle position
V	=	vehicle velocity
t	=	time
m	=	multiplier
s	=	range to target
p , q , r	=	inertial roll, pitch, and yaw rates
α	=	angle of attack
β	=	sideslip angle
ϕ	=	bank angle
$\bar{q}$	=	dynamic pressure
S	=	aerodynamic reference area
I	=	inertia
h_0	=	altitude at the start of the gravity turn
V_0	=	velocity at the start of the gravity turn
δ_r	=	rudder deflection
δ_e	=	elevon deflection
γ	=	flight path angle
μ	=	NED to body frame roll angle
ω	=	frequency

τ	=	torque
ξ	=	damping ratio
k_r	=	TAPDG trajectory shaping gain
U^a	=	aerodynamic coefficient uncertainty delta
U^m	=	aerodynamic coefficient uncertainty multiplier

REFERENCES

[1] Gavin Mendeck, Lynn Craig. "Mars Science Laboratory Entry Guidance."

[2] Brian Bihari, Michael Tigges. "Orion Capsule Handling Qualities for Atmospheric Entry," AIAA Guidance, Navigation, and Control Conference. Portland, Oregon.

[3] Tomas Martin-Mur, Gerhard Kruizinga. "Mars Science Laboratory Navigation Results."

[4] Cerimele, C., Robertson, E., Sostaric, R. (editor), Garcia, J., "A Rigid, Mid-Lift-to-Drag Ratio Approach to Human Mars Entry, Descent, and Landing," AIAA SciTech 2017, Grapevine, TX, Jan. 2017.

[5] Lu, P. "Augmented Apollo Powered Descent Guidance," In press, Journal of Guidance, Control, and Dynamics.

[6] Lu, P., "Entry Guidance: A Unified Method," Journal of Guidance, Control, and Dynamics, Vol. 37, No. 3 (2014), pp. 713-728.

[7] Lu, P., "Predictor-Corrector Entry Guidance for Low-Lifting Vehicles," Journal of Guidance, Control, and Dynamics, Vol. 31, No. 4 (2008), pp. 1067-1075.

[8] Johnson, B., Cerimele, C., Stachowiak, S., Sostaric, R., Matz, D., Lu, P., "Mid-Lift-to-Drag Ratio Rigid Vehicle Control System and Simulation for Human Mars Entry," AIAA, SciTech 2018, Kissimmee, Florida.

[9] Johnson, B., Braden, E., Sostaric, Cerimele, C., D., Lu, P., "Entry, Descent, and Landing Performance for a Mid-Lift-to-Drag ratio Vehicle at Mars," AAS, February 2018, Breckenridge, Colorado.

[10] Cherry, G. W., "A General, Explicit, Optimizing Guidance Law for Rocket-Propelled Spaceflight," AIAA Paper 64-638, 1964.